

Order-by-disorder in classical oscillator systems

F. Ionita,¹ D. Labavić,¹ M. A. Zaks,² and H. Meyer-Ortmanns¹

¹*School of Engineering and Science, Jacobs University Bremen - 28759 Bremen, Germany*

²*Institut für Mathematik, Humboldt University Berlin, 12489 Berlin Germany*

We consider classical nonlinear oscillators on hexagonal lattices. When the coupling between the elements is repulsive, we observe coexisting states, each one with its own basin of attraction. These states differ by their degree of synchronization and by patterns of phase-locked motion. When disorder is introduced into the system by additive or multiplicative Gaussian noise, we observe non-monotonic dependence of the degree of order in the system on the noise intensity: intervals of noise intensity with low synchronization between the oscillators alternate with intervals where more oscillators are synchronized. In the latter case, noise induces a higher degree of order in the sense of a larger number of nearly coinciding phases. This order-by-disorder effect is reminiscent to the analogous phenomenon known from spin systems. Surprisingly, this non-monotonic evolution of the degree of order is observed not only for a single interval of intermediate noise strength, but repeatedly as a function of increasing noise intensity.

PACS numbers: 05.45.Xt, 05.40.Ca, 64.60.aq

I. INTRODUCTION

The so-called order-by-disorder effect is usually discussed in different contexts of spin models. The term “order-by-disorder” was introduced in classical spin models [1], and it was further discussed in [2]; this effect is also observed in quantum magnetism [3, 4] and in ultracold atoms, see for example [5]. Order-by-disorder refers to the frequently found situation in which the ground state is degenerate due to competition among the interactions and this degeneracy is lifted due to disorder. Here the lifting can be temperature driven (that is entropically) [1, 4] or quantum driven as in [6] or [7, 8]. In [7, 8] this effect was studied for a two-dimensional Heisenberg antiferromagnet on a Kagomé lattice where the long-range order of spins was induced via disorder. As mentioned in [4], it depends crucially on the degree of degeneracy whether the order-by-disorder effect dominates in the competition of interactions so that its implications on correlations become visible. What makes the order-by-disorder effect particularly interesting is the feature that it appears to be counterintuitive.

In this paper we consider a different realization of an order-by-disorder effect in a system of classical active rotators [9]. Active rotators are a prototype of systems which show either limit-cycle behavior or excitable fixed-point behavior, depending on the choice of parameters. Most studies of ensembles of rotators treated attractive (positive) coupling, which favored in-phase synchronization. In a few studies a random subset of attractive couplings was replaced by repulsive ones. Disorder in the very sign of couplings was the focus of [10] with the result that a moderate fraction of repulsive interactions triggered global firing of the rotator ensemble, an effect that is suppressed for large networks unless the interaction topology is appropriately changed.

In previous work the repulsive coupling was introduced into the ensembles of active rotators [10] and Kuramoto oscillators [11] at random, without an explicit control over the induced frustration. In a recent work [12] the case of directed links was treated: for a certain proportion of oscillators (“contrarians”)

the coupling to the mean field was negative, which resulted in rich nontrivial dynamics. Differently, in this paper we consider undirected couplings and focus on effects that are merely induced by frustration and disorder in the form of additive or multiplicative noise. We therefore prescribe the sign of couplings in a way that it is possible to control the number and pattern of induced frustrated bonds and to distinguish effects generated by frustration and noise from those which owe to disorder in the coupling signs in combination with noise. As we shall see, for the latter case the order-by-disorder effect is absent. The notion of frustration in oscillatory systems was introduced by [13] and further used in [11] for Kuramoto oscillators with undirected coupling, and later generalized by one of us [14] for directed networks and excitable and oscillatory systems. In [14] we have shown that frustration in these systems can indeed lead to a considerable increase in the number of stationary states and to multistability, an effect analogous to spin systems. It is this growth in the number of coexisting attractors, for which we here introduce frustration in the active rotator systems. Without noise the system obeys gradient dynamics which drives it to lower values of potential in the high-dimensional configuration space. Evolution either ends up in one of the local minima of the energy landscape, or (since potential is not bounded from below) proceeds *ad infinitum* along the descending rifts at the bottom of landscape valleys. While the local minima in the energy landscapes of spin systems correspond to different fixed points, attractors for active rotator units, depending on the choice of parameters, can be either fixed points (minima as well) or the described rifts that, in the toroidal phase space of the system, turn into closed curves so that the motion along them corresponds to periodic oscillations. These limit cycle solutions differ by their degree of synchronization (which we call “order”): the number of *different* oscillator phases in the patterns of phase-locked motions. The more phases in the ensemble coincide in the stationary state, the higher is the order. Counterintuitively, this order can be increased via introduction into the system of disorder in the form of additive or multiplicative white noise.

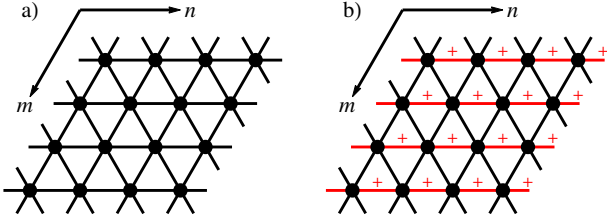


FIG. 1. Hexagonal lattice with all triangles frustrated for all couplings being negative (a) and not frustrated (b) for positive couplings along the horizontal links and negative ones otherwise.

II. THE MODEL

We study systems of N active rotators [9], whose phases φ_i are governed by the equations:

$$\frac{d\varphi_i}{dt} = \omega_i - b \sin \varphi_i + \sigma_A \xi_i(t) + \frac{(\kappa + \sigma_M \eta_i(t))}{\mathcal{N}_i} \sum_j A_{ij} \sin(\varphi_j - \varphi_i). \quad (1)$$

Here ω_i denote the natural frequencies of the rotators, b and κ parameterize, respectively, the level of excitability and the coupling strength. Further, \mathcal{N}_i denotes the number of neighbors to which the i -th unit is connected, and A_{ij} is the adjacency matrix with $A_{ii} = 0$, $A_{ij} = 1$ if $i \neq j$ and units i and j are connected, otherwise $A_{ij} = 0$. The terms $\sigma_M \eta_i$ and $\sigma_A \xi_i$ denote multiplicative and additive white noise, respectively, with $\langle \eta_i \rangle = 0 = \langle \xi_i \rangle$, $\langle \eta_i(t) \eta_j(t') \rangle = 2\delta_{ij} \delta(t - t')$, likewise $\langle \xi_i \xi_j \rangle = 2\delta_{ij} \delta(t - t')$, where σ_M and σ_A are measures for the multiplicative and additive noise intensities, respectively. Throughout the paper we set $\omega_i = \omega$ as a common natural frequency. We choose A_{ij} to represent a hexagonal lattice with periodic boundary conditions, as shown in Fig. 1 (a), so that each unit has the same number of nearest neighbors, $\mathcal{N}_i = 6$. Most former studies have been performed for positive coupling $\kappa = |\kappa|$, while we are mainly interested in repulsive coupling and choose $\kappa = -|\kappa|$. The reason is that negative κ in combination with a hexagonal coupling pattern turns all bonds into frustrated. Consider any elementary triangle formed by units i, j, k . Negative coupling ensures that unit i prefers to be antiphase to j and j prefers to be antiphase to k . As a result, i would be in phase to k , which is in conflict with the repelling direct link between them. So whatever phase the unit k assumes, the bond either between k and j or between k and i is frustrated. In order to compare our results with couplings that are disordered with respect to their sign, but do not lead to any frustrated bonds, we show also the case of positive couplings for the bonds along the horizontal directions in Fig. 1 (b), while all other bonds are repulsive.

III. MULTISTABILITY FOR REPULSIVE COUPLING

Consider eq. (1) with both sources of noise set to zero. Let us first discuss the phase space structure for $b = 0$: a set of N Kuramoto oscillators coupled on a hexagonal $(M \times L)$ -lattice. By going into the comoving frame via $\varphi(t) \rightarrow \varphi(t) - \omega t$ and rescaling the time via the normalized coupling strength $\kappa/6$ (for the given number of nearest neighbors), we arrive at

$$\dot{\varphi}_i = - \sum_j A_{ij} \sin(\varphi_j - \varphi_i). \quad (2)$$

While for positive coupling this system would have a single stable fixed point in which all phases are the same (this corresponds to synchronous oscillations with frequency ω in the lab frame), we see hints on the expected multistability for the negative coupling for a subset of solutions. These are plane-wave solutions, characterized by fronts of constant phases along parallel lines on the hexagonal lattice such that no nearest neighbors share the same phase. Their spatial distribution is characterized by

$$\varphi_{m,n} = \frac{2\pi}{M} k_1 m + \frac{2\pi}{L} k_2 n \quad (3)$$

for coordinates $m = 1, \dots, M$ and $n = 1, \dots, L$, where allowed values for the wave vector k_1, k_2 are restricted to integers by the periodic boundary conditions. For this set we prove in the appendix A.1 that for a sufficiently large extension of the lattice and an even number of the linear extension $M = L$, there are always two sets of wave vectors $k_1 = k_2 = k$ and $k_1 = k_2 = k + 1$ such that the plane waves correspond to different solutions. These solutions do not merely differ by a rotation of the linear front, but by the very number of oscillators sharing the same phase (below we denote such sets of oscillators as “clusters”).

Plane-wave solutions, which obviously reflect the lattice symmetry in their fronts of constant phases, are not the only stable solutions on a hexagonal lattice, as we shall discuss in more detail below.

In the following, without restriction of generality, we assume b to be non-negative. For $b \neq 0$, by rescaling the time unit we set $b = 1$ and follow the solutions in the parameter space of ω and κ . For $\omega < 1$ and positive κ , active rotators have a stable fixed point, $\varphi_i = \varphi_s = \arcsin \omega$, $i = 1, \dots, N$, in which all elements are synchronized with the same phase. This fixed point is stable for small negative κ as well; when κ is decreased, it loses stability via the pitchfork bifurcation at $\kappa_c = -\sqrt{1 - \omega^2}/(1 - \lambda_{\min}/\mathcal{N})$, where λ_{\min} is the minimal eigenvalue of the adjacency matrix A_{ij} . For sufficiently negative κ , when, at $\omega > 1$, every individual unit is in the limit-cycle state, there are no stable fixed points. The corresponding stability analysis is provided in appendix A.III.

Since we are primarily interested in the order-by-disorder effect, we do not further zoom into the bifurcation region, but choose κ sufficiently negative as to be well inside the parameter domain with time-dependent dynamics. This domain is characterized by

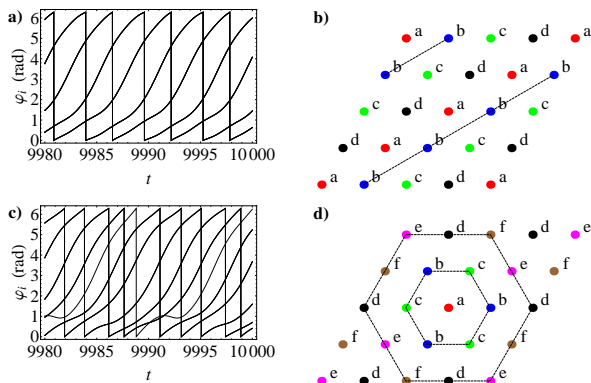


FIG. 2. Solutions of eq. (1) with 4 and 6 clusters on a 4×4 lattice for $\omega = 0.7$, $b = 1$, $\kappa = -2$ and $\sigma_M = \sigma_A = 0$.

coexisting states with different synchronization patterns. Similarly as for Kuramoto oscillators, one form of stable solutions are plane-wave patterns. They are characterized by fronts of identical phases which are parallel to each other and extend along straight lines of the hexagonal lattice as shown in Fig. 2, connecting sites which are not nearest neighbors in accordance with the repulsive couplings. Another type of solution appears as a spherical wave on a hexagonal lattice. For example, it is found as a 6-cluster solution on a 4×4 lattice. At a first glance, the phase assignments on the 4×4 -lattice, displayed in Fig. 2, look quite irregular. The characters a, \dots, f label the different clusters. However, what we see is a sector of a “discretized” spherical wave on a hexagonal lattice, with an isolated oscillator in its center, surrounded by two clusters of three oscillators, in alternating order $bc\ bc\ bc$, along the first polygon ring of nearest neighbors. In the second ring of next-nearest-neighbors of the center, we have three clusters of three oscillators, arranged like $edfedfedf$. They are plotted in Fig. 2. Phase differences within a ring and between different rings do not stay constant, but oscillate regularly.

Obviously, it depends on the lattice size and the boundary conditions whether a spherical wave matches the repulsive couplings and the concrete geometry to evolve into a stable solution.

IV. ORDER-BY-DISORDER FOR ACTIVE ROTATORS

In the following we consider active rotators coupled with frustration on hexagonal lattices of size 4×4 . First we turn on additive noise and monotonically increase its intensity. Results are shown in Fig. 3.

We plot the phases of all 16 oscillators in the interval $[0, 2\pi]$ as functions of time. While the noise intensity is varied from $\sigma_A = 0.01$ to $\sigma_A = 1$, all other parameters are kept fixed: $\omega = 0.7$, $b = 1$, $\kappa = -2$. In the presence of noise, exact coincidence of phases is washed out, but the tendency to form easily recognizable groups persists, therefore we soften the definition: we say that oscillators belong to one cluster if their phases agree within $1.6 \cdot 10^{-1}$ for $\sigma_A = 0.02$ and within $5.5 \cdot 10^{-1}$ for $\sigma_A = 0.1$, so that the ac-

curacy has to be adapted to the noise intensity. If we characterize the solutions by the cluster partitions in terms of p_n , where n denotes the number of clusters, and mark all disordered states by the symbol d , we read off the following sequence from Fig. 3: p_{16} (each oscillator is isolated) for $0 \leq \sigma \leq 0.02$; p_4 (four clusters with four oscillators in each), for $\sigma_A = 0.03$, $\sigma_A = 0.05$, and later again for $\sigma_A = 0.08$; p_6 solutions consisting of one isolated oscillator, two clusters with three oscillators each and three clusters with three oscillators each around the center of the spherical wave, for $\sigma_A = 0.06$, ($\sigma_A = 0.07$, not displayed), $\sigma_A = 0.09$ (and $\sigma_A = 0.1$, not displayed). The states as seen for $\sigma_A = 0.04$ and $\sigma_A = 0.05$ correspond to p_4 patterns, but for stronger noise the system stays in a more ordered realization of this pattern, which may give a hint on a deeper valley of the attractor in which the synchronization is less sensitive to the noise. For even stronger noise like $\sigma_A = 1.0$ the solutions get fully disordered: all phases are non-synchronized and uncorrelated. As mentioned earlier, we call the solutions the more ordered, the more phases in the ensemble synchronize. In this sense a 4-cluster solution is more ordered than a 6-cluster solution which is more ordered than a 16-cluster solution. The reason why we call the latter a clustered pattern although each cluster consists of a single oscillator, is the fact that in this state the phases are still correlated: phase differences between the sixteen oscillators oscillate periodically without noise and nearly periodically at weak noise. In contrast, in the most disordered stationary state that is observed for strong noise, the evolution of individual phases seems fully uncorrelated.

For all realizations, displayed in Fig. 3, we varied only the intensity of additive noise, starting from the same randomly chosen initial condition, and choosing the same seed for the random number generator. The question therefore arises of how representative are these plots. We formed an ensemble of hundred randomly chosen initial conditions, and for each of them we repeated the simulation with ten different realizations of noise of the same intensity. If we view as “qualitatively the same” the patterns which differ by permutations of the sequence or a different number of 6-cluster and 4-cluster solutions, then out of the hundred initial conditions $\sim 20\%$ led to qualitatively the same pattern as in Fig. 3: the sequence $(p_{16}, p_4, p_{16}, p_4, p_6, p_4, p_6, p_6, p_4, p_6, p_6, d)$. The remaining 80% of initial conditions lead to sequences like $(p_{16}, \dots, p_6, \dots, d)$ with homogeneous behavior for a larger intermediate range of noise, in case of which the non-monotonic behavior is less pronounced. From the different realizations of noise for otherwise unchanged parameters about 30% have led to qualitatively the same patterns, the actual numbers vary between one and six out of ten. We conclude that the observation of a pattern sequence displayed in Fig. 3 is not a rare event in the stochastic dynamics of the ensemble.

Similar, but visually more pronounced differences between more and less ordered and disordered states are recovered on a 10×10 -lattice. Ordered states with ten clusters of ten oscillators each are seen for the in-

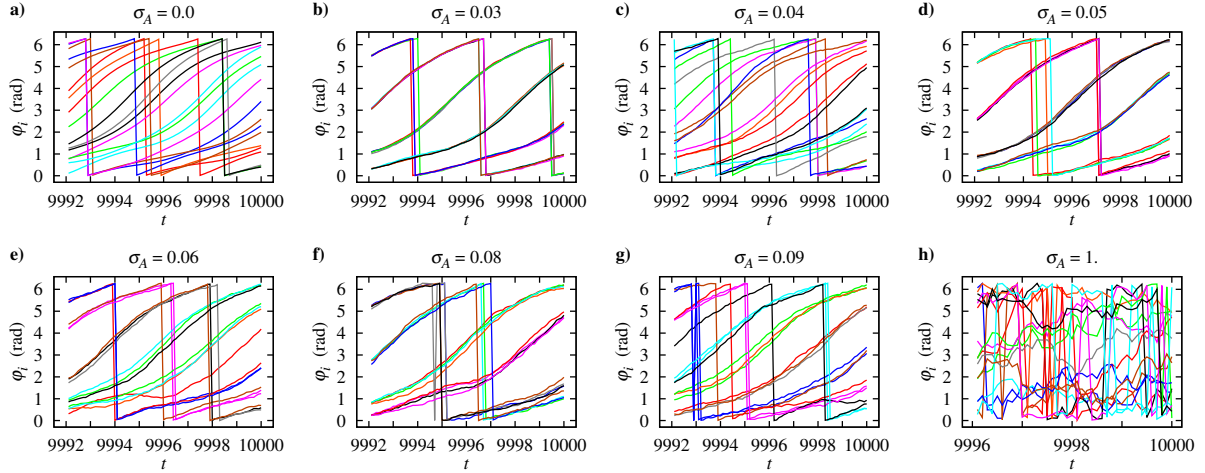


FIG. 3. Order by disorder on a 4×4 lattice, for $\omega = 0.7$, $b = 1$, $\kappa = -2$, $\sigma_M = 0$ and monotonically increasing noise intensity σ_A between panels (a) to (h). For further explanations see the text.

intermediate noise intensities $\sigma = 0.03, 0.05, 0.08, 0.09$ and 0.1 , while we see hundred different phases, synchronized for zero or small noise values and fully disordered for large noise values, for the plots see Fig. 7 in appendix A.IV.

Remarkably, if we here further zoom into the noise intervals, for example into $[0.06, 0.07]$ between the disordered patterns of hundred different phases at 0.06 and 0.07 , we see a sequence like $d o o d d d o o$, for equidistant values of σ_A between 0.061 to 0.069 , where d stands for hundred different phases and o (order) for ten different phases organized in ten clusters (Fig. 8 in appendix A.IV). At this point one may be tempted to continue the zooms to see when the characteristic order of the solutions remains the same. A variation of the noise in steps of 10^{-4} for intervals within $[0.061, 0.069]$ showed the same type of ordered solutions. However, we cannot exclude that further zooms into the resolution beyond the interval $[0.061, 0.069]$ would lead to further intermediate windows of more ordered motion.

Again, all runs for different noise intensities started from the very same randomly chosen initial conditions. Here as well a slight change in the initial conditions may lead to different patterns as function of the same increasing noise intensity. We observed similar pronounced non-monotonic behavior for about ten out of hundred different randomly chosen initial conditions.

Order-by-disorder for multiplicative noise. Similar sequences of alternating synchronization patterns as in Fig. 3 are obtained, when the additive noise is replaced by multiplicative noise and σ_M is varied between 0.01 and 0.1 , with other parameters fixed at the same values. Here we again observed the effect of order-by-disorder for roughly 10% of the different initial conditions (see Fig. 9 of appendix A.IV).

Order-by-disorder for Kuramoto oscillators. Kuramoto oscillators on the hexagonal lattice display similar sequences of states as in Fig. 3, confirming that the phenomenon is caused not by the excitability of the active rotators, but by the structure of the underlying potential landscape, which itself depends

on the lattice topology and the sign-assignments of couplings, see Figs. 10 and 11 of appendix A.IV.

V. HIERARCHIES IN THE POTENTIAL BARRIERS

We interpret the occurrence of more ordered and less ordered cluster partitions for monotonically increasing noise strength as an indication of a hierarchy in the potential barriers. In our system the role of a potential is played by the integral over φ of the equations (1), in terms of which the equations obey gradient dynamics, $d\varphi_i/dt = -\nabla_i V$, with V given by

$$V = -\omega \sum_i \varphi_i + b \sum_i \cos \varphi_i - \frac{\kappa}{2\nu} \sum_{i,j} C_{ij} \cos(\varphi_j - \varphi_i). \quad (4)$$

The first term in (4) is linear with respect to the phases φ_i and is responsible for the unbounded average drift whose slope ω is the same for all patterns. Two last terms, taken together, form the oscillatory part of the potential, V_{osc} . We evaluate V_{osc} for the 4-cluster solution, the 6-cluster solution, and the 16-cluster solution. The mean values over one period are $V_{\text{osc}}^{(4)} = -7.76$, $V_{\text{osc}}^{(6)} = -7.65$, and $V_{\text{osc}}^{(16)} = -7.51$, respectively: the higher the order, the lower the corresponding potential. However, we possess no detailed knowledge about the landscape in between, in particular about the height of the ridges. Sensitive response to different noise intensities indicates that the landscape is quite rough, owing to the implemented high degree of frustration. Numerical evidence suggests that for a sizeable portion of initial conditions, deterministic paths to their eventual attractors pass close to one or several ridges, which makes them sensitive to the action of noise and introduces uncertainty in the destination.

In general, on the very large timescale, the time evolution of φ_i under the action of noise is a walk over the entire landscape. However, for the small and moderate noise intensities the residence times in vicinities of

the deep minima or rifts are quite large (by far exceeding the computationally available times), whereas the shallow valleys are traversed relatively fast. Below we restrict ourselves to the moderately long epochs of evolution; hence, for shortness, these intermediate asymptotics near which the system spends rather long intervals of time, are referred to as “attractors”. It is these states that are displayed in Fig. 3. Furthermore, it is not the number of different patterns, characterized as p_4, p_6, p_{16} , or d , which defines the number of different attractors, since characterizations in terms of a pattern do not uniquely characterize a state due to the high degeneracy in assigning a pattern to the grid. Therefore, what we call “new attractors” below may share the same pattern as encountered before.

Consider an ensemble of stochastic trajectories which start from the same initial location in the high-dimensional landscape so that the ensemble is formed by different realizations of noise. Without noise, the gradient dynamics drives the phases along the gradient of the potential until the first local minimum or rift is met, where the system gets stuck, be it in a fixed point or in a limit cycle. Under sufficiently weak noise, the bulk of the trajectories of the ensemble remains close to the deterministic orbit and ends up at the same attracting set. Under somewhat stronger noise, the ensemble splits: part of the trajectories crosses the nearby ridge(s) and goes to different attractor(s), in contrast to the rest which follows the deterministic trajectory. This is what we have seen to occur in ten realizations. Fig. 4a) displays the temporal evolution of the oscillatory part of the potential $V_{\text{osc}}(t)$ for two trajectories which start from the same initial position under the same parameter values and correspond to two different realizations of additive noise at $\sigma_A = 0.04$. The dashed line shows the trajectory which largely follows the deterministic solution and ends up at a p_{16} pattern (the attracting state for these initial conditions in the absence of noise). The trajectory which is shown by the solid line, initially tracks the deterministic solution as well; however, after a certain time and a short epoch of strong oscillations, it appears to cross the ridge and land upon the deeper lying attractor of a p_4 solution. A closer look at the individual elements (Fig. 4 b)) shows that transitional oscillations are close to the three-clustered state: apparently this is the unstable periodic solution, located on the ridge which separates the basins of p_{16} and p_4 . The trajectory approaches this state along its stable manifold, spends some time (roughly the interval $45 < t < 75$) in its neighborhood, displaying larger amplitudes of V_{osc} , and leaves it along the unstable manifold. Very similar type of crossover behavior was found for $\sigma_A = 0.02$ and 0.03 for different noise realizations, also leading to p_4 or p_{16} patterns in the end.

Starting with yet a higher noise level, the overwhelming majority of trajectories cannot resolve the former basin of attraction any longer, as its shape gets buried under the noisy background; instead, the stronger noise enables the trajectories to explore the phase space in more remote regions from the starting point. It then depends on the depth of the valley

whether the new attractor is able to keep the trajectory in its vicinity and let the system settle inside the rift. Were the basin as shallow as the former one, the structure of the rift could not be recognized, and the transient passage of such a basin would not be identified as long-living state in our simulations.

Now our system finds repeatedly new attractors when the noise is increased. This may be either due to the presence of several ridges already in the vicinity of the starting point; it is then a random event which attractor is chosen under a new realization of noise, once its depth is sufficiently large. Or the new attractors are discovered when the noise drives the system a longer path through phase space, as long as an attractor in a more remote deep valley stops the walk. Wherever the new attractors are located, with increasing noise they have to be increasingly deep to become observable. Naturally, trajectories visiting basins of attractions between the higher ridges will be less localized for stronger noise. This feature explains the need for adapting the size of the tolerance interval within which two phases are identified, see Fig. 3 (d) and (f).

Finally and certainly, from a sufficiently large noise intensity on, the whole potential structure V is buried under the noise, and the phase trajectory performs a random walk, now driven by an effectively random potential, without correlations between individual phases, as it is seen in Fig. 3 (h).

To support these ideas we also simulated a particle in a one-dimensional potential with two barrier heights under a subthreshold external force. Accordingly, for two clearly separated noise intensities we see stochastic resonance between the frequency of switching between the attractors and the frequency of the external force. For the lower noise level, we see switching between the shallower valleys, for the larger intensity between the deeper valleys, and the particle is less localized in the deeper valleys due to the higher level of noise. The corresponding details are presented in appendix A.VI.

A. Disorder in the coupling signs, but no frustration

Without frustration, but with disorder in the coupling signs according to the choice as in Fig. 1 (b), we have neither seen a signature for multistability, nor for the order-by-disorder phenomenon in oscillators. On a 4×4 -lattice with otherwise the same choice of parameters we started from 10^6 randomly chosen initial conditions, and from 10^4 for a 10×10 -lattice. The only stationary state we have found were 2-cluster solutions with oscillators in cluster A aligned along a horizontal line and alternating with oscillators in cluster B along the succeeding horizontal line, where the phase difference between clusters A and B fluctuates about π (see Fig. 12 of appendix A.V). This shows that order-by-disorder is related to multistability, here induced via frustration.

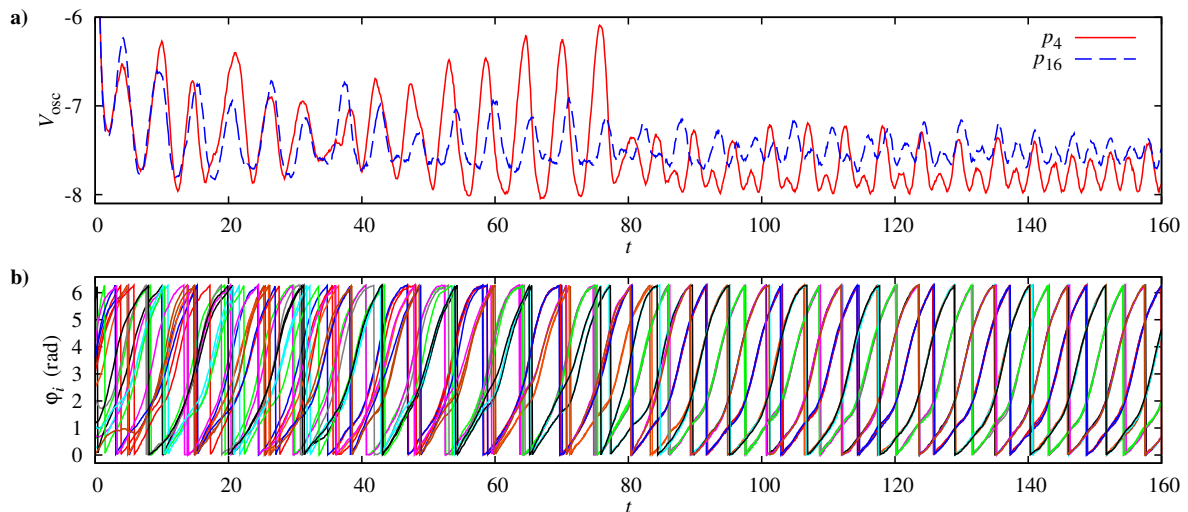


FIG. 4. a) Oscillatory component of the potential $V_{\text{osc}}(t)$ as function of time for $\omega = 0.7$, $b = 1$, $\kappa = -2$ and $\sigma_M = 0$. Two different realizations of additive noise at $\sigma_A = 0.04$. Starting from the same location with $V_{\text{osc}}(0) = -0.248$ (not displayed), two trajectories eventually go apart and end up at different attracting patterns. The dashed line tracks the deterministic solution which leads to the p_{16} -pattern. The solid line eventually leaves this path and goes to the four-cluster pattern p_4 . b) Individual phases $\varphi_i(t)$ for the solid line from the top panel. Note the proximity to the three-cluster state in the interval $45 < t < 75$.

VI. SUMMARY AND CONCLUSIONS

It is well known that the role of noise in nonlinear systems can be quite versatile [15]: in particular, it can increase the order in a disordered system. Here we made use of a similar mechanism that is known from spin systems: we have chosen the topology and the couplings in a way as to induce frustrated bonds. Frustration leads to a considerable increase in the number of attracting states. Since the units are oscillatory, coexisting states are no longer restricted to fixed points as in spin systems, but can also be different patterns of phase-locked motion. The energy landscape is not necessarily degenerate, but the system is multistable. Similarly to a number of spin systems, here the noise can also increase the order of states. Surprisingly, however, as a function of monotonically increasing noise intensity we observe not only a max-

imum of order at some optimal noise intensity, as one may have expected from analogous results on stochastic resonance [16], coherence resonance [17], or system size resonance [18]. Instead we record an alternating sequence of higher and lower order among the oscillator phases, so that the variation of the noise intensity appears to “scan” a rough potential landscape with a hierarchy of the barriers. To turn it into a practical device for scanning similar kinds of potential, the high sensitivity to the initial conditions should be reduced by adding appropriate control terms to the dynamics.

ACKNOWLEDGMENTS

Acknowledgments. Two of us (F.I. and D.L.) would like to thank the Deutsche Forschungsgemeinschaft (DFG, contract ME-1332/19-1) for financial support. M.A.Z. was supported by the DFG Research Center MATHEON (Project D21).

-
- [1] Villain J., Bidaux R., Carton J. P., Conte R., J. Phys. (France) **41**, 1263 (1980).
 - [2] Moessner R. Chalker J. T., Phys. Rev. B **58**, 12049 (1998).
 - [3] Henley C. L., Phys. Rev. Lett. **62**, 2056 (1989).
 - [4] Bergman D., Alicea J., Gull E., Trebst S. Balents L., Nature Physics **3**, 487 (2007).
 - [5] Turner A. M., Barnett R., Demler E., Vishwanath A., Phys. Rev. Lett. **98**, 190404 (2007).
 - [6] Barnett R., Powell S., Graß T., Lewenstein M. Das Sharma S., Phys. Rev. A **85**, 023615 (2012).
 - [7] Chubukov A., Phys. Rev. Lett. **69**, 832 (1992).
 - [8] Reimers J. N. Berlinsky A. J., Phys. Rev. B **48**, 9539 (1993).
 - [9] Sakaguchi H., Shinomoto S. Kuramoto Y., Prog. Theor. Phys. **79**, 600 (1988).
 - [10] Tessone C. J., Zanette D. H., Toral R., Eur. Phys. J. B **62**, 319 (2008).
 - [11] Zanette D. H., Europhys. Lett. **72**, 190 (2005).
 - [12] Hong H., Strogatz S.H., Phys. Rev. E **84**, 046202 (2011).
 - [13] Daido H., Phys. Rev. Lett. **68**, 1073 (1992).
 - [14] Kaluza P., Meyer-Ortmanns H., Chaos **20**, 043111 (2010).
 - [15] Lindner B., Garcia Ojalvo J., Neiman A., Schimansky-Geier, L., Phys. Rep. **392**, 321 (2004).
 - [16] Gammaitoni L., Hänggi P., Jung P., Marchesoni F., Rev. Mod. Phys. **70**, 223 (1998).

- [17] Pikovsky A. S. Kurths J., Phys. Rev. Lett. **78**, 775 (1997).
 [18] Toral R., Mirasso C. R. Gunton J. D., Europhys. Lett. **61**(2), 162 (2003).

APPENDIX

A.I. Multistability for Kuramoto oscillators

In the corotating reference frame the existence of steady states for Kuramoto oscillators is independent on the coupling strength, while their stability depends on the coupling sign. Here we formulate sufficient stability conditions for a certain class of fixed points, and for the coexistence of multi-stable solutions. Consider phase distributions

$$\varphi_{m,n} = \frac{2\pi}{M}k_1m + \frac{2\pi}{L}k_2n \quad (5)$$

$$m = 1, \dots, M \quad n = 1, \dots, L.$$

Obviously, for a hexagonal lattice these solutions are equilibrium points: $d\varphi_{mn}/dt = 0$.

Proposition: For negative coupling, a *sufficient* condition for the fixed points to be stable (all eigenvalues of the Jacobian are negative apart from one being zero) is given by

$$\cos\left(\frac{2\pi}{M}k_1\right) < 0, \quad \cos\left(\frac{2\pi}{L}k_2\right) < 0, \quad \cos\left(\frac{2\pi}{M}k_1 + \frac{2\pi}{L}k_2\right) < 0. \quad (6)$$

Proof: It is convenient to introduce linear labeling $i \in \{1, \dots, ML\}$ which is related to two-dimensional coordinates (m, n) , via $i = mL + n$. For normalized negative coupling as in eq. (2) of the main text, the Jacobian is given by:

$$J = \left(\frac{df_i}{d\varphi_j} \right) = \begin{cases} \sum_{k=1}^N A_{ik} \cos(\varphi_k - \varphi_i), & i = j \\ -A_{ij} \cos(\varphi_j - \varphi_i) & i \neq j. \end{cases}$$

The adjacency matrix is symmetric; the sum in each row and column equals 6, since each oscillator has six neighbors. To evaluate the Jacobian at the fixed point from eq. (5), consider the oscillator at location (m, n) with linear index $i = mL + n$. It has six neighbors located at $(m-1, n-1)$, $(m, n-1)$, $(m, n+1)$, $(m+1, n)$, $(m+1, n+1)$, and $(m+1, n+1)$, respectively; we denote their linear labels by i_1, \dots, i_6 . Hence, the row i of the Jacobian contains:

non-zero entries at columns i_1, i_2, \dots, i_6 . The J_{i,i_1} entry is

$$J_{i,i_1} = -\cos(\varphi_{i_1} - \varphi_i) = -\cos(\varphi_{m-1,n-1} - \varphi_{m,n}) = -\cos\left(\frac{2\pi}{L}k_1\right).$$

Similar calculations show that the entries at i_2, i_3, i_4, i_5 , and i_6 are, respectively:

$$-\cos\frac{2\pi}{M}k_1, -\cos\frac{2\pi}{L}k_2, -\cos\frac{2\pi}{L}k_2, -\cos\left(\frac{2\pi}{M}k_1 + \frac{2\pi}{L}k_2\right), -\cos\left(\frac{2\pi}{M}k_1 + \frac{2\pi}{L}k_2\right).$$

The diagonal element of the Jacobian J_{ii} equals minus sum of the 6 above values:

$$J_{ii} = s = \sum_{l=1}^{ML} C_{il} \cos(\varphi_l - \varphi_i) = 2 \cos\left(\frac{2\pi}{M}k_1\right) + 2 \cos\left(\frac{2\pi}{L}k_2\right) + 2 \cos\left(\frac{2\pi}{M}k_1 + \frac{2\pi}{L}k_2\right).$$

Note: The sum of entries in each row and column is zero. Hence, one eigenvalue vanishes; it corresponds to the translational invariance of the Kuramoto model. We write J as the sum of two matrices

$$J = sI + \tilde{A},$$

where I is the identity matrix and $\tilde{A}_{ij} = -A_{ij} \cos(\varphi_j - \varphi_i)$; the sum on each row of matrix \tilde{A} is $-s$. Therefore the eigenvalues of the Jacobian are

$$\lambda_J = s + \lambda_{\tilde{A}}. \quad (7)$$

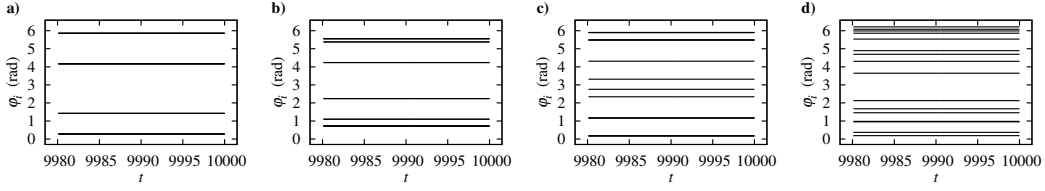


FIG. 5. Fixed point solutions with 4 clusters (a), 6 clusters (b), 8 clusters (c), and 16 clusters (d) obtained for parameter values $\omega = 0$, $b = 1$, and $\kappa = -2$.

Since \tilde{A} is symmetric, its eigenvalues are real. In accordance with the conditions in eq. (6) choose the lattice of size (M, L) and such k_1 and k_2 , that all entries of matrix \tilde{A} are positive. Then the Perron-Frobenius theorem states that all eigenvalues $\lambda_{\tilde{A}}$ of \tilde{A} fulfill:

$$\lambda_{\tilde{A}} \leq |\lambda_{\tilde{A}}| \leq \max_i \sum_j \tilde{A}_{ij} = -s \quad \Rightarrow \quad \lambda_J = s + \lambda_{\tilde{A}} \leq 0.$$

We conclude that all eigenvalues of the Jacobian are negative, besides the single vanishing one.

Next we prove a sufficient condition for the existence of multistable solutions.

Proposition: Choose $M = L$, $k_1 = k_2$, $L \geq 18$ and L even. We can then find at least two solutions of the type 5 which differ by their number of clusters.

Proof: For $k_1 = k_2 = k$, the sufficient conditions derived in eq.6 reduce to

$$\frac{2L}{8} < k < \frac{3L}{8}. \quad (8)$$

If $L \geq 18$, the interval in eq.(8) contains at least two integers. Let us consider two consecutive ones, q and $q+1$; then the associated solutions $\varphi_{m,n}^{(q)}$ and $\varphi_{m,n}^{(q+1)}$, given as

$$\varphi_{m,n}^{(q)} = \frac{2\pi}{L} q (m+n), \quad \varphi_{m,n}^{(q+1)} = \frac{2\pi}{L} (q+1) (m+n), \quad (9)$$

correspond to different numbers of clusters: Solution $\varphi_{m,n}^{(q)}$ has $L/\text{gcd}(L, q)$ clusters, where $\text{gcd}(L, q)$ is the greatest common divisor of L and q . Solution $\varphi_{m,n}^{(q+1)}$ has $L/\text{gcd}(L, q+1)$ clusters. It is straightforward to see that since L is even, $\text{gcd}(L, q) \neq \text{gcd}(L, q+1)$.

Note that these conditions are not necessary: they do not include phase distributions of spherical waves, which are numerically observed as stable solutions as well.

A.II. Multistability of fixed points for active rotators and $\omega = 0$

In the main text we focussed on multistable solutions in the oscillatory regime with coexisting solutions, which were differing by the pattern of phase synchronization. One may wonder whether we observe also multistable solutions of coexisting fixed points for active rotators. We have found such solutions for the special case of common natural frequency $\omega = 0$. These solutions can be discovered by starting from initial conditions, which are given by the known phase distributions from Kuramoto oscillators ($b = 0$) and otherwise the same choice of parameters, but then turning on b . Since we can absorb $b \neq 0$ in the time scale (setting $b = 1$), we checked the stability of these fixed point solutions under tuning κ to more negative values, keeping $\omega = 0$. Using the Newton Raphson method, we find coexisting fixed points for $\kappa < \kappa_c = -\frac{\sqrt{1}}{1 - \frac{\lambda_{\min}^A}{6}}$ (the relation for κ_c is derived below), with a supercritical pitchfork bifurcation observed at κ_c .

A.III. Stability of the fixed point, known from $\kappa = 0$, for active rotators, $\omega \neq 0$ as a function of κ

Here we discuss the solutions in the lab-frame, that is $\omega \neq 0$. Our parameter space is spanned by κ/b and ω/b for $b \neq 0$. For negative coupling we expect multistability for fixed points and/or oscillatory solutions. Along the $\omega = 0$ axis we find fixed points from the (multistable) fixed point solutions of Kuramoto systems by turning on the $-b \sin \varphi_i$ -term, as we have indicated in the previous section. Again we absorb b in the time scale (setting $b = 1$) and consider solutions in the phase space parameterized by ω and κ . Our numerical observations on the hexagonal lattices suggest that the fixed point of vanishing coupling has a large basin of attraction also for

sufficiently small positive and negative couplings, as this fixed point was the only one which we found for 10^4 different randomly chosen initial conditions for various lattice sizes (3×3 , 4×4 , 5×5 and $\omega = 0.7$) and $\kappa = -0.5$, -0.7 , -0.9 . On the other hand, for values $\kappa < -|\kappa_c|$, when $\varphi_i^{(1)}$ becomes a saddle, we always found clusters of phase locked oscillators that perform limit cycles. Therefore we derive in the following the corresponding critical (positive and) negative coupling κ_c .

For $\kappa = 0$, and $\omega < b = 1$ the equations for active rotators have $\mathcal{N} = 2^N$ fixed points, defined by $\varphi_i = \varphi_{1,2}^*$, where

$$\varphi_1^* = \arcsin(\omega), \quad \text{and} \quad \varphi_2^* = \pi - \arcsin(\omega). \quad (10)$$

Out of these \mathcal{N} fixed points, $\mathcal{N} - 2$ are saddles, one is stable, and one is unstable. The last two fixed points are located at

$$\varphi_i^{(1)} = \varphi_1^* = \arcsin(\omega) \quad (\text{stable}) \quad \varphi_i^{(2)} = \varphi_2^* = \pi - \arcsin(\omega) \quad (\text{unstable}),$$

for all $i = 1, \dots, N = M \cdot L$. The location of these two fixed points in phase space is independent of the value of κ . Next we derive how the stability properties of $\varphi_i^{(1)}$ and $\varphi_i^{(2)}$ change when $\kappa \neq 0$. Evaluating the corresponding Jacobian J at these two fixed points we obtain at $\varphi_i = \varphi_1^* = \arcsin(\omega)$

$$J_1^* = \begin{cases} -\sqrt{1-\omega^2} - \kappa, & i = j \\ \frac{\kappa}{\nu} A_{ij} & i \neq j \end{cases} \Rightarrow J_1^* = \frac{\kappa}{\nu} A - (\sqrt{1-\omega^2} + \kappa) I,$$

where $\nu = 6$ for six nearest neighbors on the hexagonal lattice. If λ_i^A are the eigenvalues of the adjacency matrix, then the eigenvalues of J_1^* are

$$\lambda_i^{(1)} = \frac{\kappa}{6} \lambda_i^A - \kappa - \sqrt{1-\omega^2}. \quad (11)$$

For $\kappa = 0$, the fixed point φ_1^* is stable, since all eigenvalues of J_1^* are negative. For $\kappa < 0$, the first eigenvalue λ_i that becomes positive corresponds to the smallest eigenvalue of A , λ_{\min}^A , provided $\lambda_{\min}^A < 6$ with $\nu = 6$ (otherwise all $\lambda_i < 0$, for all $\kappa < 0$). The transition takes place at

$$\kappa_c = -\frac{\sqrt{1-\omega^2}}{1 - \frac{\lambda_{\min}^A}{6}}. \quad (12)$$

Evaluated at the second fixed point from eq. (10), $\varphi_i = \varphi_2^* = \pi - \arcsin \omega$, J becomes:

$$J_2^* = \begin{cases} \sqrt{1-\omega^2} - \kappa, & i = j \\ \frac{\kappa}{6} A_{ij} & i \neq j \end{cases} \Rightarrow J_2^* = \frac{\kappa}{6} A - (-\sqrt{1-\omega^2} + \kappa) I.$$

The eigenvalues of J_2^* are

$$\lambda_i^{(2)} = \frac{\kappa}{6} \lambda_i^A - \kappa + \sqrt{1-\omega^2}. \quad (13)$$

For $\kappa = 0$, the fixed point φ_2^* is unstable, since all eigenvalues of J_2^* are positive.

For $\kappa > 0$, the first eigenvalue λ_i that becomes negative corresponds to the smallest eigenvalue of A , λ_{\min}^A , provided $\lambda_{\min}^A < 6$ (otherwise all $\lambda_i > 0$, for all $\kappa > 0$.) The transition takes place at

$$\kappa_c = \frac{\sqrt{1-\omega^2}}{1 - \frac{\lambda_{\min}^A}{6}}. \quad (14)$$

For our hexagonal lattice, the maximum eigenvalue $\lambda_{\max}^A = 6$. Therefore we conclude: as we increase κ to $\kappa > 0$, the fixed point $\varphi^{(1)}$ remains stable since $\lambda_i^{(1)} < 0$; the fixed point $\varphi^{(2)}$ becomes a saddle at a critical value $\kappa_c^+ = \sqrt{1-\omega^2} / \left(1 - \frac{\lambda_{\min}^A}{6}\right)$.

For $\kappa < 0$, the fixed point $\varphi^{(2)}$ remains unstable, with all eigenvalues $\lambda_i^{(2)} > 0$; the stable fixed point $\varphi^{(1)}$ loses stability and becomes a saddle at a critical value

$$\kappa_c = -\frac{\sqrt{1-\omega^2}}{1 - \frac{\lambda_{\min}^A}{6}}. \quad (15)$$

In the vicinity of the bifurcation regime. Oscillatory behavior in the immediate vicinity of κ_c is shown in Fig. 6. While some units perform full-circle rotations, a few others (in this case just one unit, labeled by a), display small amplitude oscillations. Moving off the bifurcation region, all units proceed to rotation.

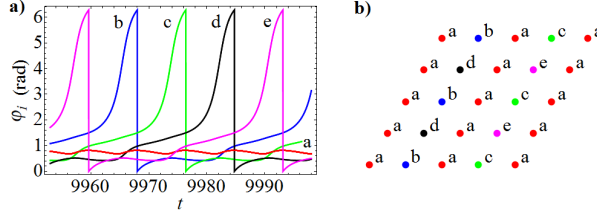


FIG. 6. Solutions with 5 clusters, on a 4×4 lattice for parameter values $\omega = 0.7$ $b = 1$, and $\kappa = 1.01\kappa_c = -0.5356$.

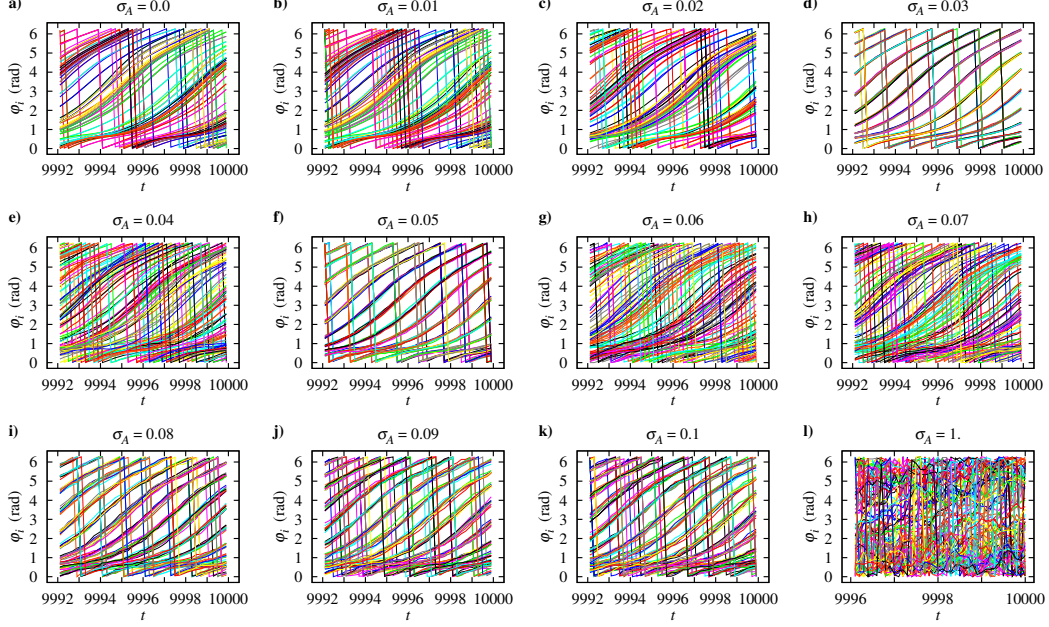


FIG. 7. Order by disorder on a 10×10 lattice, for parameter values $\omega = 0.7$ $b = 1$, and $\kappa = -2$.

A.IV. Supplementary figures to the main text

Order-by-disorder for 10×10 lattices and additive noise. Here we present the plots for a 10×10 lattice (Fig. 7), including a further zoom into the noise interval between 0.061 to 0.069 in Fig. 8, as mentioned in the main text.

Order-by-disorder for 10×10 lattices and multiplicative noise. Figure 9 illustrates practical equivalence of additive and multiplicative noise with respect to the order-by-disorder effect. This is not unexpected: the multiplicative noise proportional to σ_M adds a further term to the “coupling part” in eq. (1) of the main text.

Order-by-disorder for Kuramoto oscillators and additive noise. The plots of Fig. 10 illustrate that excitability of active rotators is not essential for the order-by-disorder effect: the figures look qualitatively very much like those for active rotators.

A.V. No order-by-disorder for disorder in the coupling signs

In Fig. 12 we demonstrate absence of the order-by-disorder effect when the coupling signs are arranged according to Fig. 1 (b) of the main text. Without frustrated bonds for otherwise the same choice of parameters, instead of multistability there is a single attracting pattern as in Fig. 12 for all 10^6 tested initial conditions.

A.VI. Analogy with stochastic resonance

As an argument in favor of our conjecture of a hierarchical landscape with potential barriers of various depths, we demonstrate analogous behavior for stochastic resonance. To this aim we choose a one-dimensional potential $U(x)$ with only two levels of barriers: $U(x) = \sum_{i=1}^4 \alpha_i x^{2i}$, as shown in Fig. 13 (a). Unlike most studies of stochastic resonance, we are interested not in temporal (resonance-like) aspects of dynamics, but in localization of solutions in different basins.

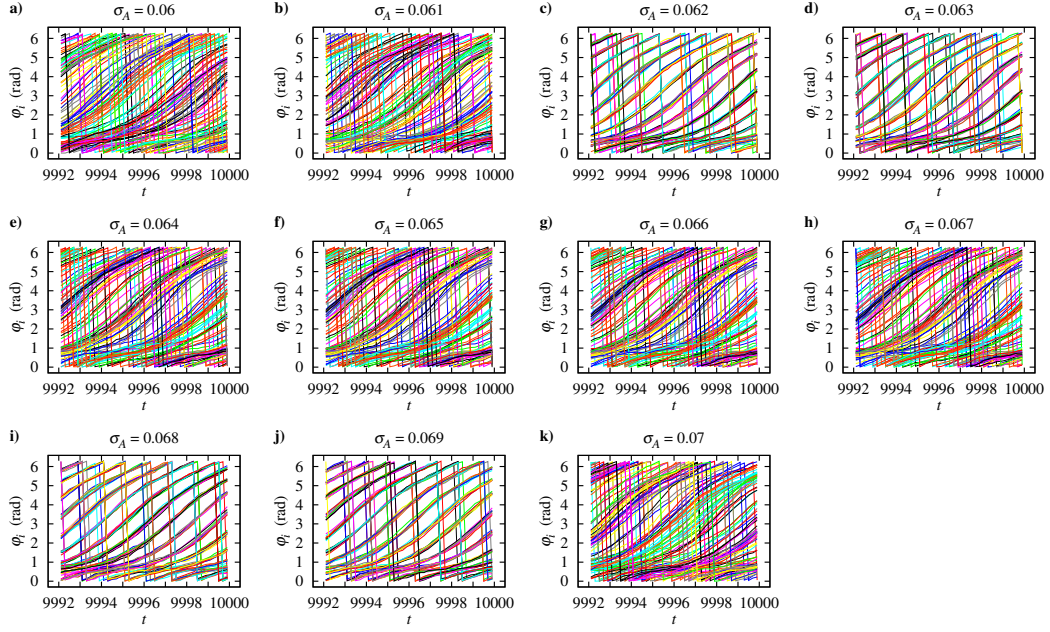


FIG. 8. Zoom into the noise interval between 0.061 to 0.069, for otherwise the same parameters as in Fig. 7.

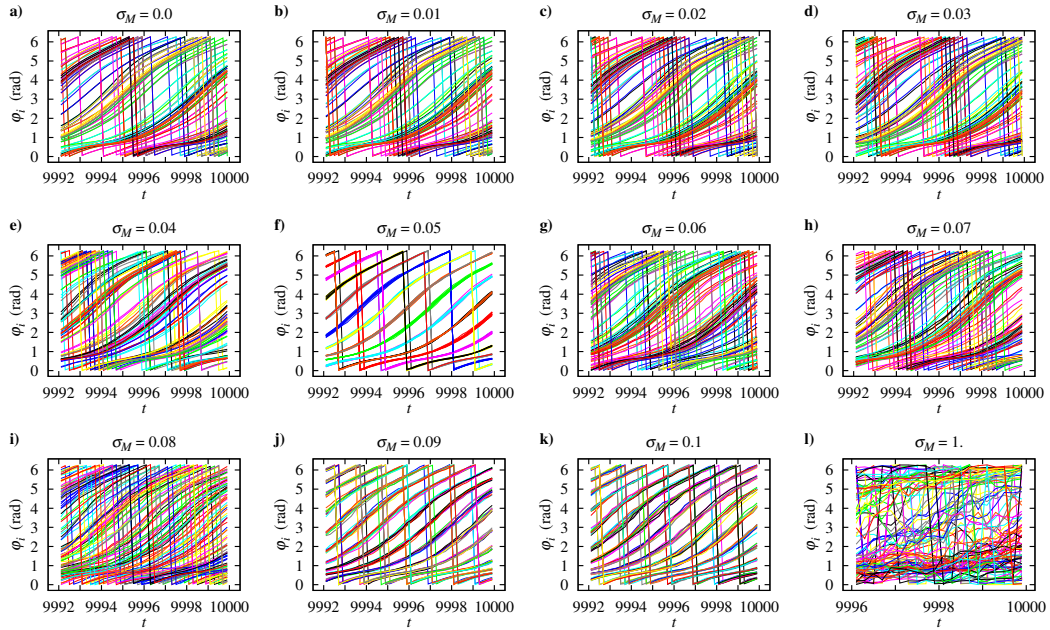


FIG. 9. Same as Fig. 7, but for multiplicative noise.

Consider the motion of a particle, described by the stochastic differential equation

$$\frac{dx}{dt} = -\frac{dU}{dx} + A \sin \omega t + \xi(t), \quad (16)$$

where $\xi(t)$ is Gaussian white noise with intensity σ : $\langle \xi(t) \rangle = 0$, $\langle \xi(t)\xi(t') \rangle = 2\sigma\delta(t-t')$. An external subthreshold periodic perturbation $A \sin \omega t$ does not allow the particle to leave any of the four local minima in the absence of noise, but combined with noise it triggers the switching between different minima. In Fig. 13 (b)-(f) the response of the system to increasing noise intensity σ is shown. For low intensity ($\sigma = 0.22$), we observe very small random oscillations about one of the local minima, here about $x = 1$ (Fig. 13 (b), red line). Regular oscillations in Figs. 13 (b)-(f) show the periodic external force (blue lines). For an optimal noise strength ($\sigma \simeq 0.53$), the particle is enabled to cross the lower barrier, so it jumps in resonance with the external frequency ω between $x = 1$ and $x = 2$ (or, depending on the initial conditions, $x = -1$ and $x = -2$) (Fig. 13 (c)). For an intermediate larger noise intensity the motion between $x = 1$ and $x = 2$ is irregular (Fig. 13 (d)). For crossing the second

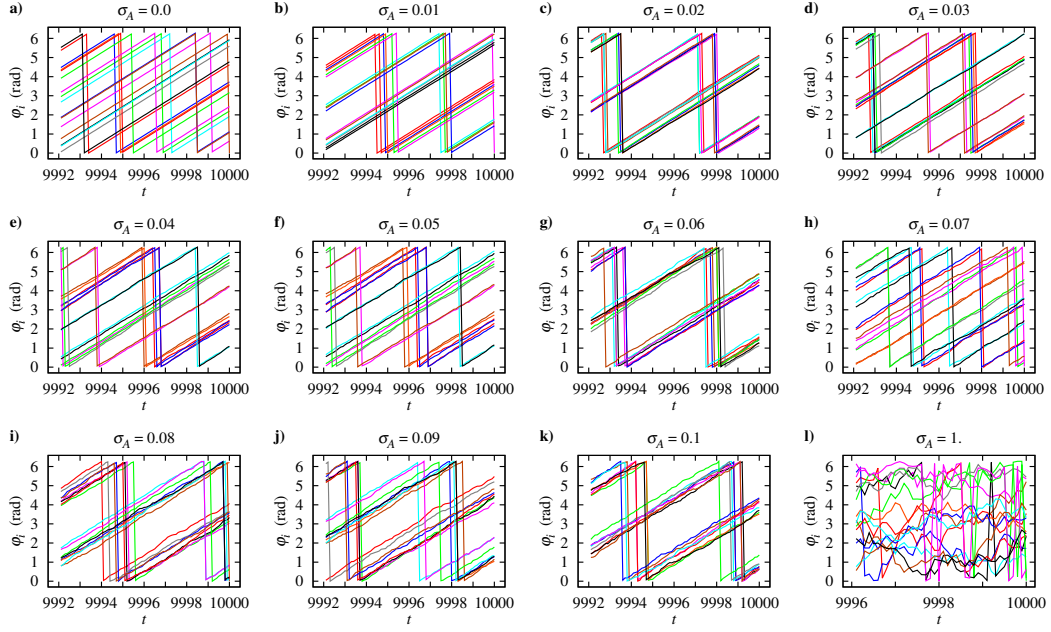


FIG. 10. Same as Fig. 7, with $b = 0$ (Kuramoto oscillators) on a 4×4 lattice.

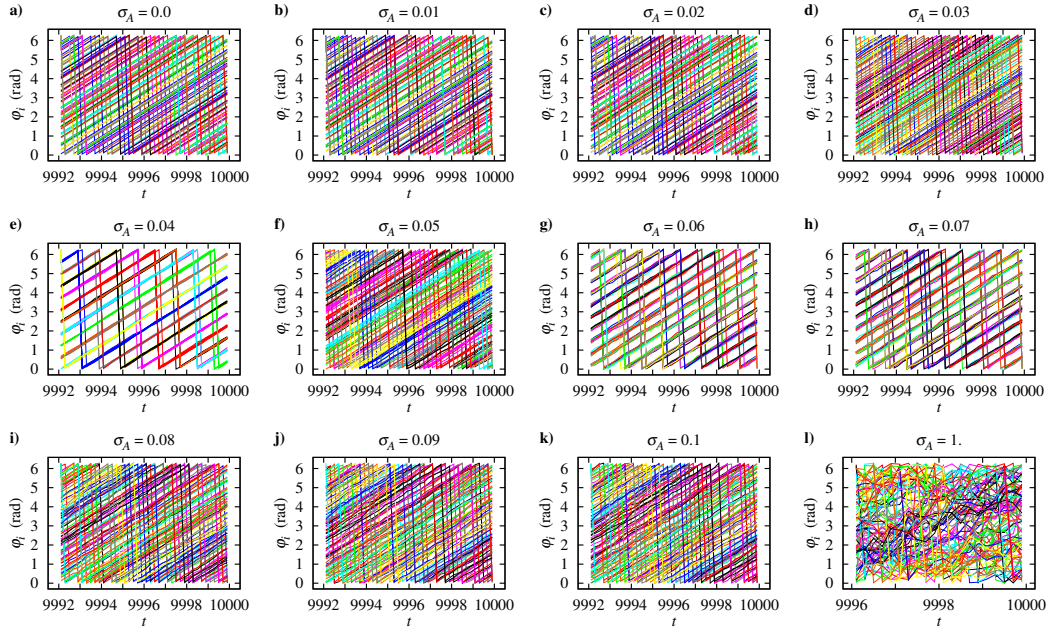


FIG. 11. Same as Fig. 7, but for Kuramoto oscillators with $b = 0$ on a 10×10 lattice.

barrier, there is the second “optimal” noise strength $\sigma \simeq 1.22$ for which the particle jumps in resonance with the external frequency between locations in the interval $[1, 2]$ and $[-2, -1]$ (Fig. 13 (e)). For even larger noise the particle does no longer see the underlying shape of the potential, but moves irregularly between the outer walls (Fig. 13 (f)). We see that under higher noise intensity the localization occurs on levels separated by higher barriers, and the particle is less localized in the vicinity of the minima. This reduced localization is akin to our need for adapting the tolerance interval when two rotator phases are identified within $\pm \Delta\varphi$.

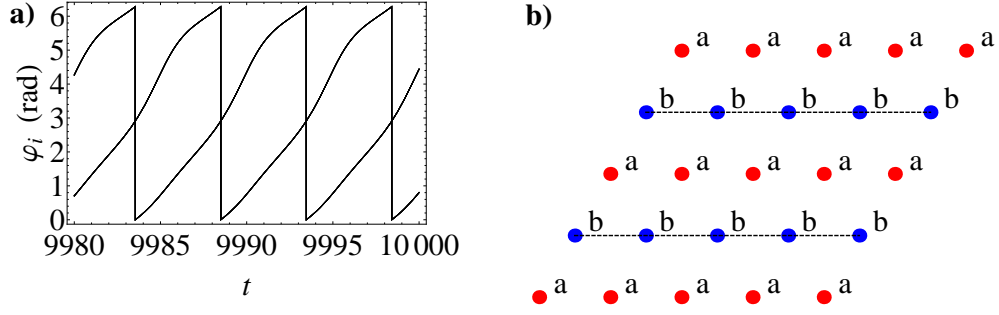


FIG. 12. Two-cluster solution on a 4×4 lattice without frustration. Oscillators in cluster a and b share the same phase, respectively. The solution is representative for our results for $\omega = 0.7$, $b = 1$, and $\kappa = -2$ and 10^6 randomly chosen initial conditions.

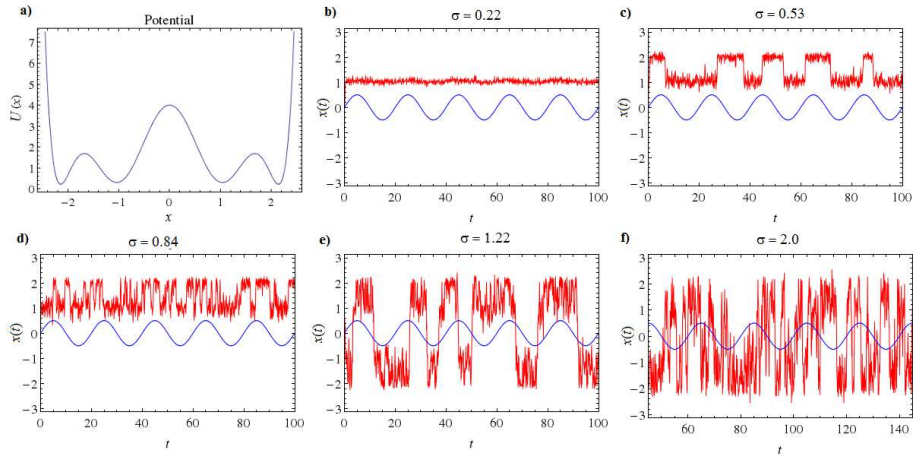


FIG. 13. Stochastic resonance for a potential (a) with two barrier heights: Panels (b) - (f) show the value of the force (in blue) and the response of the system (in red) as functions of time, for different noise intensities $\sigma = 0.22, 0.53, 0.84, 1.22$, and 2.0 . For further explanations see the text.